Multiphase *LLC* Resonant Converter With Natural Current Sharing and Phase-Shedding

Ubaid Ahmad, *Student Member, IEEE*, Roberto Giral, *Senior Member, IEEE*, Carlos Olalla, *Member, IEEE*, Ariya Sangwongwanich, *Member, IEEE*, Pooya Davari, *Senior Member, IEEE*, and Frede Blaabjerg, *Fellow, IEEE*

***Abstract*—The multiphase *LLC* converter is commonly used for high-power and high step-down applications. However, the tolerances in the tank circuit parameters cause uneven current sharing (CS), reducing system reliability. Additionally, phase-shedding (PS) can improve converter efficiency at partial load by turning-OFF phases. This paper proposes a multiphase input-parallel output-parallel *LLC* resonant converter with a common inductor-capacitor branch, with the objective to achieve excellent CS and phase-shedding at the same time. Thanks to the shared branch, current-sharing is natural, and phase-shedding is realized without affecting the operating point. With fewer passive components and a simple phase connection, the design offers low-cost, high-power density, and improved light-load efficiency compared to existing solutions. Detailed analysis shows improved CS on both the primary and secondary sides, when compared to previous approaches. Simulation and experimental results for the proposed two-phase *LLC* resonant converter validate the analysis and illustrate the effectiveness of the CS and PS capabilities. At the rated load of 800 W, CS error is 2.48% on the primary side and 2.0% on the secondary side. Phase-shedding improves efficiency by 3.60% at 50% load and 6.82% at 25% load.**

***Index Terms*—Multiphase *LLC* resonant converter, natural current-sharing, phase-shedding, efficiency, and power density.**

I. Introduction

THE *LLC* resonant converter is a promising solution for data centers, communications supplies, and electric vehicle battery chargers, among others, due to its zero-voltage and zero-current switching capabilities, which achieves high efficiency and power density [1], [2], [3]. However, in high-power or high output current applications, the current stress on the secondary side and the bulky filter capacitor limits the use of the *LLC* converter. To alleviate the current stress and reduce the filter size, the *LLC* converter can be adapted to the input-parallel output-parallel (IPOP) configuration [4], [5], [6], [7], [8], [9], [10], [11], [12], [13], [14], [15], [16], [17], [18], [19], [20], [21], [22], [23], [24], [25], [26], [27], [28]. Nonetheless, small differences in the gain of the resonant tanks in IPOP circuits result in uneven current distribution. These experimental discrepancies in the gains of the resonant tanks are unavoidable, and are caused by tolerances in the resonant capacitors, inductors, and magnetizing inductances. Other mismatches are avoidable or relatively minor by comparison, such as differences in the ON-resistance of the switches, mismatches in the gate signals, and other uneven path resistances and parasitic. These mismatches result in significant power imbalances within the IPOP converters. Uneven current or power distribution can lead to the over-dimensioning of components, increased thermal stress on devices, and degraded reliability of the IPOP converters.

To tackle this issue, many techniques have been proposed, including control-based current-sharing (CS) methods [4], [5], [6], [7], such as variable frequency control [8] and phase-shift control [9]. Active CS methods, which use switch-inductor and switch-capacitor techniques, have also been explored [10], [11]. Alternatively, passive CS approaches include magnetics-based techniques [12], [13], [14], [15], [16], [17] capacitive-based methods [18], [19], and grouping the secondary windings of transformers [20], along with an improved version of this method [21]. CS based on virtual voltage sources is another passive strategy [22]. Furthermore, the output filter has been used to achieve balanced current-sharing, with common *CL* and/or *CLC* filter-based methods presented in [23], [24]. Passive impedance matching techniques can also achieve CS [25], employing a common inductor (*CI*) [26], a common capacitor (*CC*) [27], or a unified common inductor and common capacitor (*UCICC*) [28]. Each of these methods has its own advantages and drawbacks, which are discussed below.

Control-based current-sharing techniques [4], [5], [6], [7] rely on complex control schemes and additional sensing or conditioning circuits, which increase the cost and complexity of IPOP resonant converters. For example, the method in [6] uses extra partial power processing DC-DC converters to achieve balance currents. Similarly, variable frequency and phase-shift controls

Received 11 September 2024; revised 17 December 2024; accepted 27 January 2025. Date of publication 25 February 2025; date of current version 9 July 2025. Paper 2024-IPCC-1356.R1, presented at the 2024 IEEE Applied Power Electronics Conference and Exposition, Long Beach, CA, USA, Feb. 2529, and approved for publication in the IEEE TRANSACTIONS ON INDUSTRY APPLICATIONS by the Industrial Power Converter Committee of the IEEE Industry Applications Society [DOI: 10.1109/APEC48139.2024.10509208]. This work was supported in part by the European Union Horizon 2020 through the Marie Sklodowska-Curie under Grant 945413 and in part by Universitat Rovira i Virgili. *(Corresponding author: Ubaid Ahmad.)*

Ubaid Ahmad, Roberto Giral, and Carlos Olalla are with the Department of Electrical Electronics and Automatic Control Engineering, School of Electrical and Computer Engineering, Universitat Rovira i Virgili, Països Catalans, 26 43007 Tarragona, Spain (e-mail: ubaid.ahmad@urv.cat; roberto.giral@urv.cat; carlos.olalla@urv.cat).

Ariya Sangwongwanich, Pooya Davari, and Frede Blaabjerg are with the Department of Energy, Aalborg University, 9220 Aalborg, Denmark (e-mail: ars@et.aau.dk; pda@energy.aau.dk; fbl@energy.aau.dk).

Color versions of one or more figures in this article are available at https://doi.org/10.1109/TIA.2025.3544983.

Digital Object Identifier 10.1109/TIA.2025.3544983

TABLE I
COMPARISON OF THE PROPOSED CONVERTER AND EXISTING MULTI-PHASE *LLC* RESONANT CONVERTERS

Principle of CS	Control Based		Magnetic Integration (MI) Based				Capacitor CB Based	Common *LC* or *CLC* Filter Based	Common Connection Based			**Proposed Method**
	[8]-[9]	[10]-[11]	[20]	[22]	[14]	[15]-[17]	[18]-[19]	[23]-[24]	[26]	[27]	[28]	-
CS Performance	Very Good	Good	Good	Excellent	Very Good		Excellent	Very Good	Good	Poor	Good	**Excellent**
PS Ability	-	YES	NO				NO	NO	NO			**YES**
Converter Complexity	Fairly High	Fairly High	Fairly High (complexity of HF magnetic design)				High	High	Low	Low	High	**Low** (simple one connection)
Added Components Cost	High (costly sensors & conditioning circuits)	High (additional switches & driver circuits)	High (additional secondary windings)		High (additional CS cells)	Low (MI of existing inductors)	High (additional costly film capacitors)	High (additional cost of added *LC* & *CLC* filters)	Low (simple one or more connections with no additional components)			**Fairly Low** (reduced cost with common *LC* branch)
Light-Load Efficiency	-	High	Low		Low	Low	Low	Low	Low			**High**

CS→current-sharing, PS→phase-shedding, HF→high frequency, CB→charge balance.

in [8], [9] adjust the load currents in real time but require costly sensors and intricate control systems, which can compromise system stability.

Active CS methods using the switch-capacitor or switch-inductor techniques [10], [11] control the inductance or capacitance of the resonant tanks. However, they require extra switches, gate drivers, passive components, and a complex control system. As a result, these methods can reduce power density and increase system cost.

Passive current-sharing methods based on magnetics are explored in [12], [13], [14], [15], [16], [17]. In [12], three balancing transformers compensate for component tolerances, enabling even current-sharing in a three-phase *LLC* resonant converter. Similarly, [13] introduces a spatial magnetic core-based current balancing transformer, but these approaches require customized cores, increasing cost and complexity. An alternative method uses magnetic coupling current balancing cells in IPOP *LLC* modules [14]. With CS cells, this method adds resonant inductors, increasing magnetic volume and cost while reducing power density. To address this, an integrated current balancing transformer (ICBT) based CS is proposed in [15], [16], [17]. By coupling existing resonant inductors, the ICBT achieve current balancing while providing sufficient impedances for inductive operation in *LLC* modules. An improvement is introduced in [16], where integrated current balancing cells for a bidirectional *CLLC* resonant converter ensure even CS on both the primary and secondary sides. Unlike other methods, the CS cells in [16], effectively realizes the even CS on the secondary side of the converter, while other approaches addressing assumptions that good primary CS guarantees good secondary CS. The concept of coupled inductors has also been applied in other contexts, such as voltage balancing in dual-output resonant triple-active-bridge converters for bipolar DC distribution systems [29].

Another passive CS approach for *LLC* converters employs the idea of charge balance in capacitors [18], [19]. In [18], an additional flying capacitor is used in a two-phase *LLC* converter. Similarly, two flying capacitors are added to achieve CS in an asymmetric three-phase system in [19]. The idea in [19] is an extension of [18]. However, extending the topology to more than three or four phases is not recommended due to the design difficulties of asymmetric resonance operation. Moreover, it increases the cost of the IPOP converters due to the additional expensive film capacitors required in the circuit.

In [20], [21], grouping the secondary windings of the transformers has been proposed. However, asymmetric leakages on the secondary sides impair the CS performance in [20]. This issue is addressed in [21] with an improved grouping of the secondary windings. However, placing additional module requires three additional windings on the transformers secon- dary sides. This degrades power density and efficiency while increasing complexity and cost. Additionally, it complicates transformer manufacturing and limits system scalability. Since all modules are coupled, removing a module is also challenging. In [22], a CS method using virtual controllable voltage sources is introduced. It adds an auxiliary winding to each phase module, inserting it into the resonant tank of another phase and balancing currents by controlling the phase-shift angle between phases. However, this requires extra windings in each phase—two per phase when there are more than three modules—hence further increasing system complexity and cost. In [23], [24], a common *CL* and/or *CLC* filter is presented for two-phase and five-phase systems. These common filters provide different impedance under mismatched conditions, enabling even current sharing. However, they require additional passive components on the load side, which reduces power density, efficiency, and increases cost.

Finally, the impedance matching method is proposed in [25]. As mentioned earlier, *CI* [26] and *CC* [27] circuits achieve current-sharing by determining the impedance matching points connection between two-phases. However, these methods still require improvements for both primary and secondary side CS. A common capacitor only addresses discrepancies in resonant capacitors, while a common inductor mitigates mismatches in resonant inductors. In summary, the impedance matching techniques in [25], [26], [27] offer simple solutions for utilizing *LLC* converters in IPOP configurations. However, *CC* and *CI* methods exhibit high CS errors on the secondary side, and the *CI* method introduces high current ripple on filter capacitors due to premature turn-ON of one rectifier. Additionally, these methods cannot improve light-load efficiency by enabling phase-shedding (PS). To reduce CS errors further, the *UCICC* circuit introduced in [28] utilizes common connections for both inductors and capacitors. Although this approach reduces CS errors, it increases system complexity with additional connections between phases. Moreover, *UCICC* cannot fully implement PS under light-load conditions, resulting in lower efficiency for multi-phase converters.

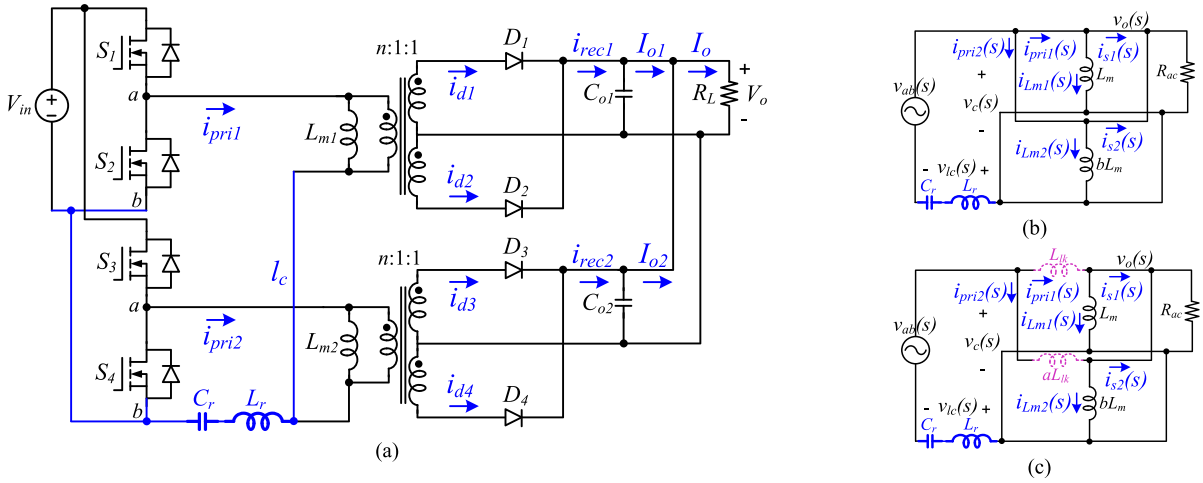

Fig. 1. (a) Proposed two-phase *LLC* resonant converter, (b) AC equivalent circuit without, and (c) with transformer leakage inductances.

The different methods have been classified and compared in Table I, with respect to the CS sharing principle. The literature discusses qualitative CS performance [30]; however, this paper quantifies the CS performance into the categories based on CS error percentage, such as, excellent (0–3%), very good (3–5%), good (5–10%), and poor (>10%). Note that not all methods achieve a good combination of features. Some achieve excellent and/or very good CS, but with added component count, related cost, and complexity. Others remain simple (connection-based) but exhibit worse CS capabilities. In addition, none of them feature phase-shedding to improve the multiphase converter light-load efficiency except [10], [11]. However, they achieve good CS performance with the expense of additional switches and its related driving circuitry.

In comparison to the methods discussed, this paper proposes a multiphase *LLC* resonant converter using a common inductor-capacitor (*LC*) branch between phases, achieving excellent current-sharing and phase-shedding. The detailed comparison in Table I shows the advantages of the proposed method [31].

In general, and in comparison, to the common connection-based CS methods using *CI*, *CC* and *UCICC* circuits [26], [27], [28], the proposed converter, depicted in Fig. 1(a), exhibits the following desirable features:

1) The resonant tanks in the proposed two-phase *LLC* converter require only two passive components (one capacitor and one inductor).
2) Compared to the *UCICC* method, the points of connection in the resonant tank elements are reduced from three to one, which simplifies the system.
3) The proposed converter can achieve PS ability, in contrast with the *CI*, *CC*, and *UCICC* methods. Specifically, when compared to the *CI* and *CC* methods, the resonance frequency of the proposed converter does not change when one of the phases is turned-OFF. Hence, the gain and the high efficiency operating point of the converter remain unchanged.
4) Since the proposed method uses the single *LC* branch for two-phases, mismatches in the resonant tanks are eliminated, ensuring natural current sharing. In contrast, existing CS techniques strive to mitigate these mismatches for better CS performance.
5) Excellent CS in the center-tapped rectifiers of individual converters is demonstrated experimentally by adopting bi-filar winding techniques. This automatically eliminates the discrepancy caused by asymmetric secondary and tertiary leakages of the transformer, an imbalance not discussed in [26], [27], [28].

The paper is organized as follows: Section II discusses the proposed two-phase *LLC* resonant converter. Section III presents the current-sharing performance of the proposed method. Section IV shows the phase-shedding capabilities of the proposed approach. Sections V and VI discuss the simulation and experimental results of the proposed converter and compare them with existing technologies. Section VII concludes the paper.

II. Proposed Two-Phase *LLC* Resonant Converter

The circuit diagram of the proposed two-phase *LLC* resonant converter is depicted in Fig. 1(a). The circuit consists of half-bridges on the primary sides (four active switches), a common *LC* branch (L_r, C_r) with a single point of common connection (l_c), two high-frequency center-tapped transformers with turns ratio (n), a full-wave rectifier for each phase of the converter, requiring a total of four diodes (D_1, D_2, D_3, D_4), and two filter capacitors (C_{o1}, C_{o2}). The proposed common *LC* branch based two-phase *LLC* converter has some good benefits compared to the existing technologies, which are listed in the previous section. In addition, the *LLC* modules can be easily removed or added except the common *LC* branch, when required.

III. Current Sharing Ability of the Proposed Converter

A. Current-Sharing Disregarding Leakage Inductances

The AC equivalent circuit of the proposed converter, assuming no leakage inductances of the main transformer and C_{o1}, C_{o2} are large value capacitors, is shown in Fig. 1(b). In this case, it could be considered that the leakages are small and/or that

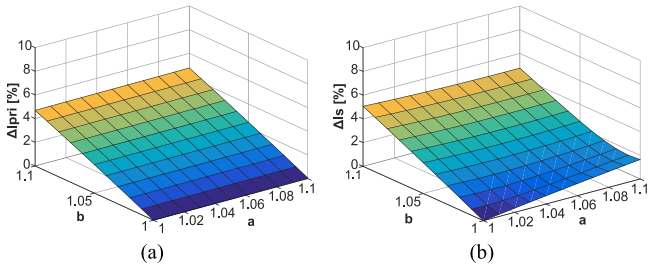

Fig. 2. CS error (a) primary side ΔI_{pri}, and (b) secondary side ΔI_s.

they are equivalent. Thus, they would have no effect on the current sharing performance and the primary currents would be balanced. Although the primary side currents would be balanced, the secondary currents could still be different because of the mismatches in the magnetizing inductances of the main transformers. With these mismatches, the secondary side currents would be $i_{s1} = i_{pri1} - i_{Lm1}$ and $i_{s2} = i_{pri2} - i_{Lm2}$. Given that $i_{pri1} = i_{pri2}$, the difference is caused by i_{Lm1} and i_{Lm2}, which could be quantified as follows:

$$\Delta I_s = \left| \frac{i_{Lm2} - i_{Lm1}}{i_{Lm1} + i_{Lm2}} \right| \% \tag{1}$$

B. Current-Sharing Considering Leakage Inductances

In practice, the leakage inductances of the main transformer are not zero and exhibit mismatches. Together with the differences in magnetizing inductances, these mismatches are defined as two factors noted a and b, accounting for the differences between phases 1 and 2, as follows:

$$\begin{cases} L_{r1} = L_{r2} = L_r \\ C_{r1} = C_{r2} = C_r \\ L_{lk1} = L_{lk} \quad L_{lk2} = aL_{lk} \\ L_{m1} = L_m \quad L_{m2} = bL_m \end{cases} \tag{2}$$

where subscripts 1 and 2 denote phases 1 and 2, respectively.

The AC equivalent circuit of the proposed converter, assuming leakage inductances of the main transformer, is shown in Fig. 1(c). The load resistance R_L can be expressed in terms of the output voltage V_o and the total output power P_o, as $R_L = V_o^2 / P_o$. Thus, the ac equivalent load resistance reflected to the primary side of the converter can be expressed as follows:

$$R_{ac} = \frac{8n^2}{\pi^2} R_L \tag{3}$$

where, n is the turns ratio of the transformer. Since the mismatches of L_r and C_r are naturally eliminated, the transfer function from the point of common connection $V_c(s)$ to the output of the converter $V_o(s)$ can be obtained as follows:

$$H\ (s) = \frac{\frac{1}{sL_{lk}} + \frac{1}{saL_{lk}}}{\frac{1}{sL_{lk}} + \frac{1}{sL_m} + \frac{1}{saL_{lk}} + \frac{1}{sbL_m} + \frac{1}{R_{ac}}} \tag{4}$$

where, $H\ (s) = \frac{V_o(s)}{V_c(s)}$.

Using Kirchhoff's current law (KCL) in Fig. 2(c), the load currents including the effects of L_{lk}, L_m and aL_{lk}, bL_m can be written as:

$$I_{s1}\ (s) = \frac{V_c\,(s)}{sL_{lk}} - \frac{V_o\,(s)}{sL_{lk}} - \frac{V_o\,(s)}{sL_m} \tag{5}$$

$$I_{s2}\ (s) = \frac{V_c\,(s)}{saL_{lk}} - \frac{V_o\,(s)}{saL_{lk}} - \frac{V_o\,(s)}{sbL_m} \tag{6}$$

where, $I_{s1}(s)$ and $I_{s2}(s)$ are the secondary or load side currents of individual modules. Using (4) and re-arranging (5) and (6) results in:

$$I_{s1}\ (s) = \frac{V_c\,(s)}{sL_{lk}} \left[1 - H\,(s) \left(1 + \frac{L_{lk}}{L_m} \right) \right] \tag{7}$$

$$I_{s2}\ (s) = \frac{V_c\,(s)}{saL_{lk}} \left[1 - H\,(s) \left(1 + \frac{aL_{lk}}{bL_m} \right) \right] \tag{8}$$

Finally, the load current sharing error can be obtained using (7) and (8) and Table III, which is given by:

$$\Delta I_s = \left| \frac{I_{s2} - I_{s1}}{I_{s1} + I_{s2}} \right| \% \tag{9}$$

Similarly, the relationship of the primary currents using KCL in Fig. 1(c) can be written as:

$$\begin{cases} I_{pri1}\ (s) = I_{Lm1}\ (s) + I_{s1}\,(s) \\ I_{pri2}\ (s) = I_{Lm2}\ (s) + I_{s2}\,(s) \end{cases} \tag{10}$$

The solution of these currents is obtained using (7), (8) and (10) and given by:

$$I_{pri1}\ (s) = \frac{V_c\,(s)}{sL_{lk}}\ [1 - H\,(s)] \tag{11}$$

$$I_{pri2}\ (s) = \frac{V_c\,(s)}{saL_{lk}}\ [1 - H\,(s)] \tag{12}$$

Thus, the transformer primary current sharing error (ΔI_{pri}) can be obtained using (11) and (12), which is defined as:

$$\Delta I_{pri} = \left| \frac{I_{pri2} - I_{pri1}}{I_{pri1} + I_{pri2}} \right| \% \tag{13}$$

In summary, the percentage current sharing error on the primary as well as on the secondary or load side of the converters can be obtained in the case of mismatches in the leakage and/or magnetizing inductances. Both sets of equations, (7) and (8) for the load side, (11) and (12) for the primary side, show that when $a = 1$, and $b = 1$ (perfect matched condition) the current sharing error on the primary as well as on the secondary side is zero percent, which corresponds to perfect current sharing. Fig. 2 shows the percentage error in the primary side (a) and in the secondary or load side (b) for mismatches up to $\pm 10\%$of the nominal value. Hence, with $a = 1.1$, and $b = 1.1$, the proposed FHA model results the maximum primary CS error of $\Delta I_{pri} = 4.5\%$, and a secondary CS error of $\Delta I_s = 4.6\%$, both of which increase linearly with mismatches.

IV. Phase-Shedding Ability of the Proposed Converter

In general, phase-shedding is applied to multiphase converter systems when operating at or below 50% of the rated load to improve efficiency. Not all multiphase converters offer this ability, as mentioned previously and as shown in Table I.

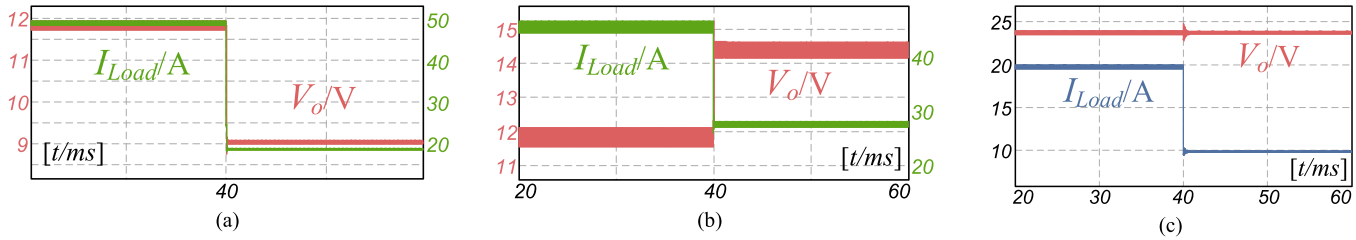

Fig. 3. Simulation results of (a) *CC* [27], (b) *CI* [26], and (c) *UCICC* [28] methods, showing V_o and I_{Load} with phase-shedding at 40 msec.

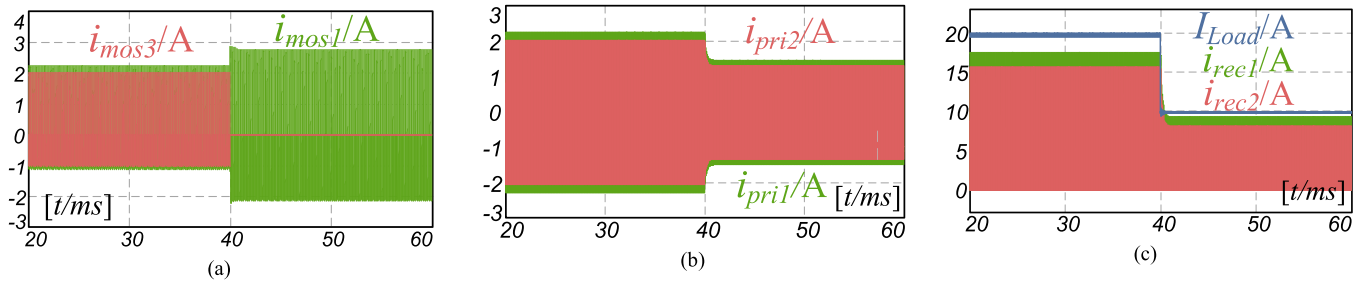

Fig. 4. Simulation results of *UCICC* [28] method when phase 2 turned-OFF at 40 msec, (a) top side MOSFETs currents of phase #1 and #2 (i_{mos1}, i_{mos3}), (b) transformer primary currents (i_{pri1}, i_{pri2}), (c) rectifier currents (i_{rec1}, i_{rec2}) of module #1 and #2.

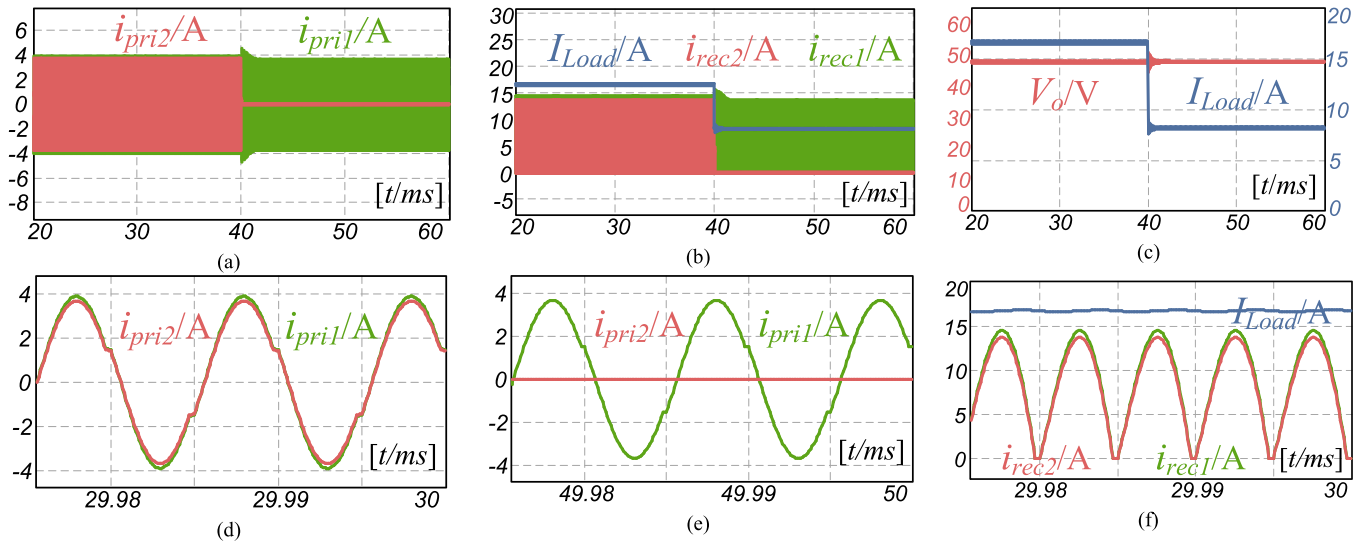

Fig. 5. Simulation result of the proposed converter with phase-shedding at 40 msec, (a) transformer primary currents (i_{pri1}, i_{pri2}), (b), rectifier currents and total load current (i_{rec1}, i_{rec2}, I_{Load}), (c) V_o and I_{Load}, (d), (e) i_{pri1}, i_{pri2} before and after phase-shedding, (f) i_{rec1}, i_{rec2}, and I_{Load} before phase-shedding.

For example, in the case of the *CI* and *CC* current-sharing methods [26], [27], when module 2 switches S_3 and S_4 are turned OFF, the common elements of the tank circuit are connected in parallel, and the resonance of the tank circuit shifts to new frequencies, as follows:

$$f_{r,CI} = \frac{1}{2\pi\sqrt{(L_{r1}//L_{r2})\,C_{r1/2}}} = \sqrt{2}\,f_r \tag{14}$$

$$f_{r,CC} = \frac{1}{2\pi\sqrt{(C_{r1}+C_{r2})\,L_{r1/2}}} = \frac{f_r}{\sqrt{2}} \tag{15}$$

where $f_{r,CI}$ and $f_{r,CC}$ are the resonance frequencies of the *CI* and *CC* methods after phase-shedding. These changes in the resonance of the tank circuit mean that the operating point is different, when considering a constant switching frequency. The voltage gain, and hence the output voltage of the converter, are greatly affected, which is undesirable. Therefore, phase-shedding with the *CI* and *CC* circuits becomes impractical.

The change in the resonance point issue is solved in the *UCICC* circuit [28], where both the inductor and capacitor are connected in parallel when module 2 switches S_3 and S_4 are turned OFF. The resonance of the tank circuit remains

TABLE II
CURRENT-SHARING AND PHASE-SHEDDING PERFORMANCE COMPARISON

***CC* Method [27]**						**Phase-Shedding**	**Inductor (*I*), Capacitor (*C*)**
Load Power	**Phases**	$i_{pri,rms}$	$\Delta i_{pri,rms}$	$i_{rec,avg}$	$\Delta i_{rec,avg}$		
600 W	Phase #1	2.469 A	6.01 %	27.569 A	10.85 %	No	2***I***, 2***C***
	Phase #2	2.189 A		22.170 A			
***CI* Method [26]**							
		$i_{pri,rms}$	$\Delta i_{pri,rms}$	$i_{rec,avg}$	$\Delta i_{rec,avg}$		
600 W	Phase #1	2.125 A	5.4 %	28.290 A	5.6 %	No	2***I***, 2***C***
	Phase #2	2.369 A		31.635 A			
***UCICC* Method [28]**							
		$i_{pri,rms}$	$\Delta i_{pri,rms}$	$i_{rec,avg}$	$\Delta i_{rec,avg}$		
480 W	Phase #1	1.575 A	5.31 %	10.476 A	5.96 %	No	2***I***, 2***C***
	Phase #2	1.416 A		9.298 A			
Proposed Method							
		$i_{pri,rms}$	$\Delta i_{pri,rms}$	$i_{rec,avg}$	$\Delta i_{rec,avg}$		
800 W	Phase #1	2.692 A	2.51 %	8.579 A	2.82 %	Yes	1***I***, 1***C***
	Phase #2	2.560 A		8.107 A			

TABLE III
PARAMETERS OF THE PROPOSED CONVERTER

Parameters	**Phase #1**	**Phase #2**
Resonant inductor (L_r)	45.5 μH	
Leakage inductances (L_{lk1}, L_{lk2})	4.11 μH	4.5 μH
Resonant capacitor (C_r)	47 nF	
Magnetizing inductance (L_{m1}, L_{m2})	320.5 μH	352 μH
Input voltage (V_{in})	380 V	
Switching frequency (f_{sw})	100 kHz	
Transformer turns ratio (n)	4 : 1	
Output voltage (V_o)	48 V	
Total output power (P_o)	800 W (400 W per phase)	
Transformer cores	PQ3535, N97	
Inductor core	RM14, N97	
Primary switching devices	UJ3C065080T3S	
Rectifier diodes	SBR20A150CT	

the same after phase-shedding, as defined by the following equation:

$$f_{r,UCICC} = \frac{1}{2\pi\sqrt{(L_{r1}//L_{r2})\,(C_{r1}+C_{r2})}} = f_r \qquad (16)$$

where $f_{r,UCICC}$ is the new resonance frequency after phase-shedding. Although $f_{r,UCICC}$ equals f_r, the currents still flow in the resonant tank of phase 2 due to the connections between the resonant tank circuits on the primary sides of the transformers. Thus, the current in the transformer windings and on the secondary (load) side remains shared. This means that the *UCICC* method lacks full phase-shedding capability and fails to enhance light-load efficiency.

In contrast to the methods discussed, the proposed circuit maintains the same resonance frequency after phase-shedding, as demonstrated in the following equation:

$$f_r = \frac{1}{2\pi\sqrt{L_r C_r}} \qquad (17)$$

Since the resonance frequency remains the same, so does the voltage gain. This ensures the same high efficiency operating point during phase-shedding. The voltage gain of the proposed converter remains comparable to that of the conventional *LLC* converter, both before and after phase-shedding. Therefore, the gain can be derived, as presented in [15].

V. SIMULATIONS RESULTS AND COMPARISON

A simulation study is performed to compare the CS and PS capabilities of the proposed converter with those of existing technologies, including the *CC* method [27], the *CI* method [26], and the *UCICC* method [28]. The circuits of the *CC*, *CI*, and *UCICC* methods have been simulated in PSIM with the parameters and power ratings provided in [26], [27], [28]. The proposed converter has been simulated with the parameters and Case 1 mismatches provided in Table III. It should be noted that the total number of mismatched conditions, considering about 10% tolerances in leakage and magnitizing inductances, could be $2^2 = 4$, which are as follows:

Case 1: L_r, C_r, $L_{lk2} = 1.10 \times L_{lk1}$, $L_{m2} = 1.10 \times L_{m1}$
Case 2: L_r, C_r, $L_{lk2} = 0.90 \times L_{lk1}$, $L_{m2} = 1.10 \times L_{m1}$
Case 3: L_r, C_r, $L_{lk2} = 1.10 \times L_{lk1}$, $L_{m2} = 0.90 \times L_{m1}$
Case 4: L_r, C_r, $L_{lk2} = 0.90 \times L_{lk1}$, $L_{m2} = 0.90 \times L_{m1}$

The worst-case among these four conditions defined in [15], [16] are Case 1 and Case 4. This is due to the circuit parameters deviating in the same direction, which creates higher CS error compared to the other two cases. Therefore, Case 1 among the worst-cases is considered for simulation and experiment.

The rms primary currents ($i_{pri,rms}$) and the rectifier average currents ($i_{rec,avg}$) for all methods are listed in Table II. The simulation results of the *CC* and *CI* methods are shown in Figs. 3(a), (b). In both cases, it can be seen from the waveforms of the output voltage and the total load current (V_o, I_{Load}) that when the load is halved (at 40 ms) and phase 2 is turned OFF, the operating point of the converter changes and the output voltage is disturbed, which is not desirable. In the case of the

CC method, the resonance changes following (15), as discussed in Section IV. This new operating point is above the nominal resonance point, so that the output voltage changes from 12 V to 9 V. Similarly, in the case of the *CI* method, the operating point follows (14). The new operating point after phase-shedding is below the nominal resonance point, so that the output voltage shifts from 12 V to 14.3 V. Moreover, based on the transformer primary rms currents and the rectifier average currents of the constituent modules, the percentual current-sharing errors in the *CC* method are $\Delta\, i_{pri,rms} = 6.01\%$, and $\Delta\, i_{rec,avg} = 10.86\%$. In the *CI* method, the CS errors are $\Delta\, i_{pri,rms} = 5.4\%$, and $\Delta\, i_{rec,avg} = 5.6\%$.

Also, the *UCICC* method has been simulated with the parameters and the power rating given in [28]. Phase-shedding is applied to the circuit when the load is halved at 40 ms. Fig. 3(c) shows the total load current and output voltage (V_o, I_{Load}). It can be seen from the figure that the output voltage remains the same during phase-shedding. As explained in Section IV and given in (16), the operating point remains unchanged. However, the *UCICC* method cannot achieve complete phase-shedding. Although the current of the MOSFETs in phase 2 becomes zero after turning-OFF S_3 and S_4, as shown in Fig. 4(a) (where $i_{mos3} = 0$ A after 40 ms), the transformer primary windings as well as the rectifiers are still sharing currents, as depicted in Figs. 4(b), (c). Therefore, due to the connections of the resonant tank, it is observed that the *UCICC* cannot achieve complete phase-shedding, hence showing a limited improvement in light-load efficiency. Regarding the current-sharing error, the *UCICC* method results in a primary current sharing error of $\Delta\, i_{pri,rms} = 5.31\%$, and a rectifier current sharing error of $\Delta i_{rec,avg} = 5.96\%$.

Finally, the proposed circuit is simulated with the parameters listed in Table III, with the aim to verify the CS and PS performance of the proposed converter. Fig. 5 shows the simulation results with phase-shedding at 40 ms when the load is reduced to one half. Figs. 5(a), (b) and (e) show the currents in phase 2 when S_3 and S_4 are turned-OFF. First, it can be seen that the currents i_{pri2} and i_{rec2} are equal to zero after 40 ms. Secondly, Fig. 5(c) shows how the operating point remains the same and the output voltage remains unchanged. Then, the current-sharing performance can be verified from the zoomed-in waveforms in Figs. 5(d) and (f). The CS error in the primary currents is $\Delta\, i_{pri,rms} = 2.51\%$, and the CS error in the rectifier currents is $\Delta i_{rec,avg} = 2.82\%$. First, these errors are consis- tently better than those of the previously proposed approaches. Secondly, the results are in reasonable agreement with the predictions of the simplified FHA model shown in Section III. Moreover, the proposed converter requires only one inductor and one capacitor in the tank circuit, whereas the other methods require two inductors and two capacitors. Thus, the proposed converter can improve the power density and reduce the cost of the multiphase *LLC* converter.

VI. Experimental Results

A hardware prototype has been designed and built to demonstrate the effectiveness of the proposed method. The *LLC* converter in phase #1 is used as a reference and is noted module #1.

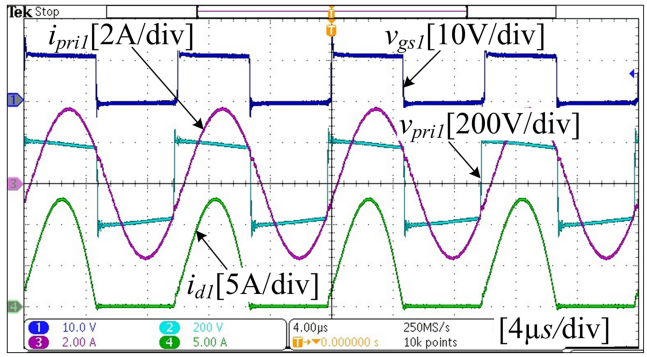

Fig. 6. Experimental result of single *LLC* converter with 400 W.

First, module #1 is tested at a power rating of 400 W. Then, the combined power rating of the proposed two-phase *LLC* converter has been verified at 800 W. The mismatches (about 10%) in the second *LLC* module (phase 2) are intentionally introduced with respect to module #1, aiming to produce a mismatch in the resonant tank elements and to show the current sharing performance of the proposed converter in the worst-case (Case 1). The parameters of the two-phases are given in Table III.

A. Single LLC Converter

Fig. 6 shows the experimental results of the single *LLC* module #1 with a power rating of 400 W. The results include the gate-to-source signal (v_{gs1}) of MOSFET S_1, the transformer primary current (i_{pri1}), the primary winding voltage (v_{pri1}), and the rectifier diode current (i_{d1}). The results are consistent with zero-voltage-switching (ZVS) operation for the primary inverter side and with zero-current-switching (ZCS) for the diode rectifiers of the converter. Thanks to these features, a peak efficiency of 94.1% is achieved at full load.

B. Conventional Two-Phase LLC Converter

To show the imbalance in the currents in the conventional two-phase *LLC* converter, a second module has been designed and fabricated with a mismatch in tank circuit parameters of 10% compared to module #1. Since it can be expected that the power is to be delivered only by module #1, the tests are limited to a power rating of 400 W, the maximum power capability of a single *LLC* module. Fig. 7 shows the experimental results of the conventional two-phase *LLC* converter, where Fig. 7(a), (b) show the transformer primary currents (i_{pri1}, i_{pri2}), diode rectifier currents i_{d1}, and i_{d4} in Fig. 7(a), and i_{d2}, and i_{d3} in Fig. 7(b) . It can be seen from the waveforms that the diode rectifier currents in module #2 are $i_{d3} = 0$ A, and $i_{d4} = 0$ A, while i_{d1} and i_{d2} are responsible for delivering all the power to the load. On the primary side of the converter, the transformer primary current in module #2 (i_{pri2}) is the magnetizing current circulating in the primary side of the converter, while i_{pri1} is responsible for delivering power to the load. Therefore, it is evident that the mismatches in the tank circuit create significant imbalances in the currents and make the multiphase converter unreliable. This is a serious safety issue for the converters connected in parallel,

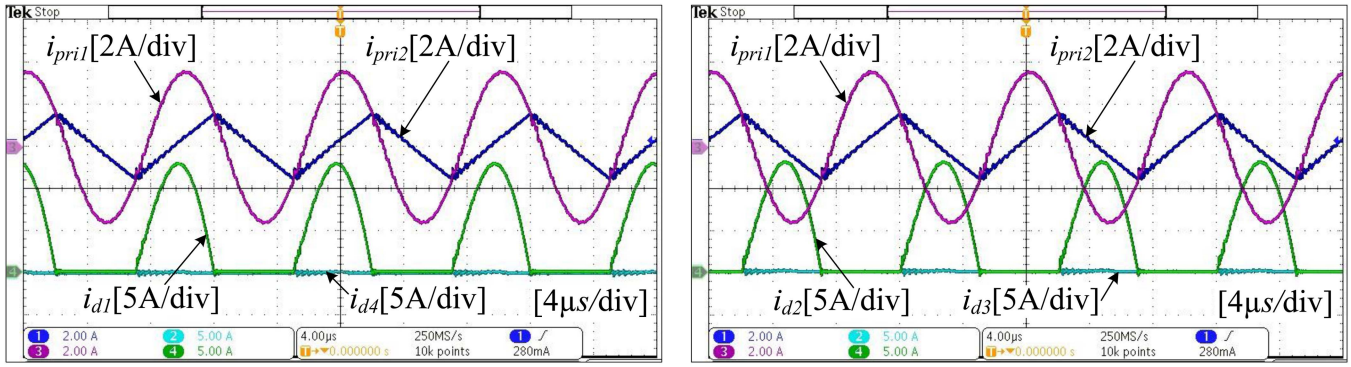

Fig. 7. Experimental results of conventional two-phase *LLC* converter, (a) transformer primary currents (i_{pri1}, i_{pri2}) and diode rectifier currents (i_{d1}, i_{d4}), (b) transformer primary currents (i_{pri1}, i_{pri2}) and diode rectifier currents (i_{d2}, i_{d3}).

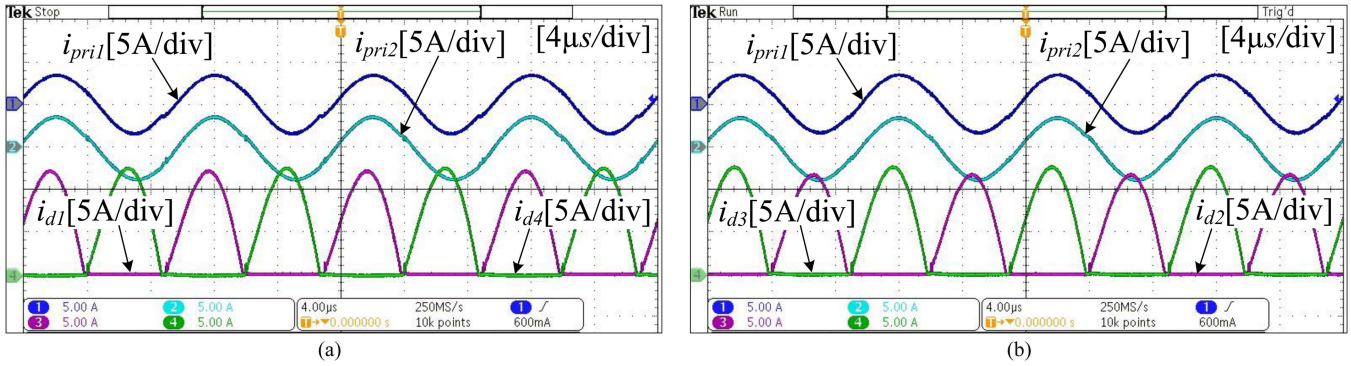

Fig. 8. Experimental results of the proposed two-phase *LLC* converter with full-load condition (800 W), (a) transformer primary currents (i_{pri1}, i_{pri2}) and diode rectifier currents (i_{d1}, i_{d4}), (b) transformer primary currents (i_{pri1}, i_{pri2}) and diode rectifier currents (i_{d2}, i_{d3}).

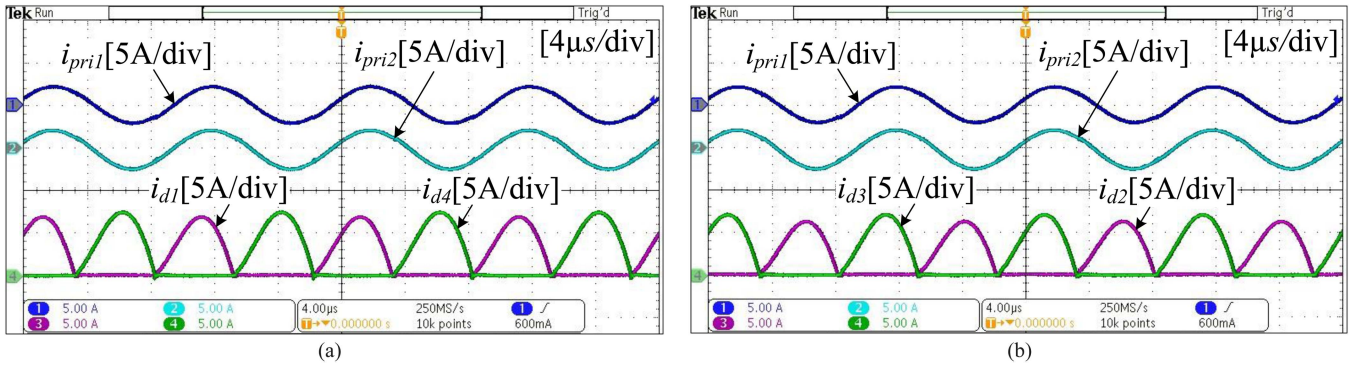

Fig. 9. Experimental results of the proposed two-phase *LLC* converter with half-load condition (400 W), (a) transformer primary currents (i_{pri1}, i_{pri2}) and diode rectifier currents (i_{d1}, i_{d4}), (b) transformer primary currents (i_{pri1}, i_{pri2}) and diode rectifier currents (i_{d2}, i_{d3}).

TABLE IV
CURRENT-SHARING AND PHASE-SHEDDING PERFORMANCE OF THE PROPOSED CONVERTER

Proposed Converter Current-Sharing Performance							**Phase-Shedding**
Load Power	**Phases**	$i_{pri,rms}$	$\Delta i_{pri,rms}$	$i_{d1/d4,avg}$	$i_{d2/d3,avg}$	Δi_{avg}	
100 % Load (800 W)	Phase #1	2.199 A	2.48 %	3.639 A	3.649 A	$\Delta i_{d1/d4,avg} = 1.58$ %	Yes
	Phase #2	2.311 A		3.756 A	3.798 A	$\Delta i_{d2/d3,avg} = 2.0$ %	
50 % Load (400 W)	Phase #1	1.612 A	2.77 %	2.028 A	1.987 A	$\Delta i_{d1/d4,avg} = 3.56$ %	
	Phase #2	1.525 A		2.178 A	2.200 A	$\Delta i_{d2/d3,avg} = 5.08$ %	

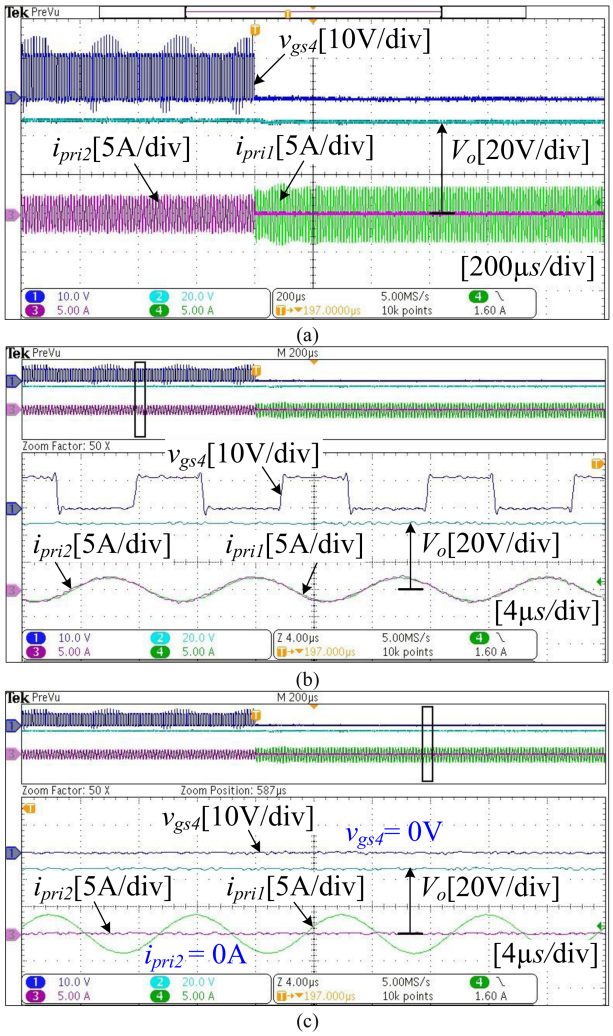

Fig. 10. Experimental results of the proposed two-phase *LLC* converter with phase-shedding under half-load condition, (a) primary currents (i_{pri1}, i_{pri2}), gate-to-source voltage of switch S_4 (v_{gs4}), and output voltage (V_o), (b) zoom-in waveforms of (a) before PS, and (c) after PS.

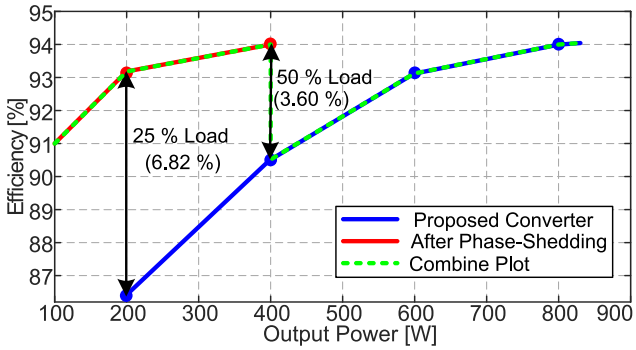

Fig. 11. Efficiency plot of the proposed converter.

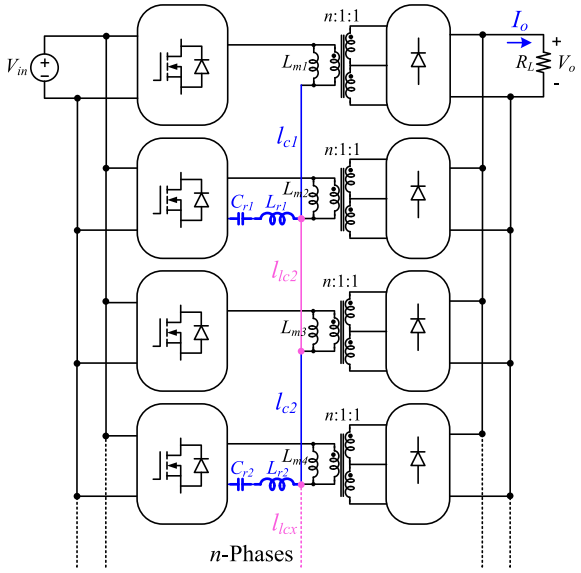

Fig. 12. Extension of the proposed converter to *n*-phases.

which is addressed with the proposed method in the following subsection.

C. CS of the Proposed Converter At Full-Load and Half-Load

The experiments showing the performance of the proposed two-phase common *LC* branch-based *LLC* converter are explained here. As introduced in Section III, the proposed converter eliminates the mismatches in the main tank circuit parameters except for the mismatches in the transformer magnetizing inductances (L_{m1}, L_{m2}) and leakage inductances (L_{lk1}, L_{lk2}). To demonstrate the good current-sharing ability of the proposed converter with mismatches in these parameters, intentional mismatches of about 10% in the magnetizing and leakage inductances have been inserted in the transformers, as defined in Case 1. These mismatches correspond to the factors "*a*" and "*b*", according to the CS model discussed in Section III in (2), where $L_{lk2} = aL_{lk}$ and $L_{m2} = bL_m$.

The experimental results of the proposed converter under full-load condition are depicted in Fig. 8. First, Fig. 8(a) shows the transformer primary currents (i_{pri1}, i_{pri2}) and the rectifier diode currents of the two modules (i_{d1}, i_{d4}). Then, Fig. 8(b) also shows the transformer primary currents, but with the other two rectifier diode currents (i_{d2}, i_{d3}). It can be seen that, with the proposed technique, the currents are equally shared between the two modules, which makes the parallel-connected two-phase *LLC* converter more reliable. Although the currents seem to be very well shared, we present the mean values (i_{avg}) of the rectifier diode currents and the rms values (i_{rms}) of the transformer primary currents in Table IV. The values have been measured using a Tektronix MDO3014 oscilloscope. Also, the difference in mean values between modules #1 and #2 (diodes 1, 4 and diodes 2, 3 are compared) has been derived. The results are very valuable because they show the current-sharing performance with respect to the existing technologies.

It can be seen that, under full-load conditions, the current sharing error in the primary side of the converter is $\Delta\, i_{pri,rms} = 2.48\%$. On the secondary side, it is $\Delta i_{d1/d4,avg} = 1.58\%$ in diodes 1 and 4, whereas it is $\Delta i_{d2/d3,avg} = 2.0\%$ in diodes 2 and 3. Thus, the maximum difference in the rectifier currents is

2.0% and in the primary side currents is 2.48%. These values reflect an excellent CS in the proposed converter. Besides, there is a small, negligible difference between the rectifier currents of modules #1 and #2, which mainly depends on the asymmetry in the secondary and tertiary windings of the transformer. This factor has been minimized by using a bifilar winding arrangement similar to that in [32]. This technique minimizes the asymmetry of center-tapped rectifiers and, therefore, allows for the calculation of the correct percentage error between the rectifier currents of the two modules.

The performance of the proposed converter has been verified under half-load (50%) conditions. The experimental results are shown in Fig. 9. First, Fig. 9(a) shows the transformer primary currents i_{pri1} and i_{pri2}, along with the diode rectifier currents i_{d1} and i_{d4}. Similarly, Fig. 9(b) shows the difference in the primary currents, but with the rectifier currents of the other two modules: i_{d2} and i_{d3}. Again, the rms vales for the primary currents and the mean values for the rectifier diodes are listed in Table IV. The results show that, under half-load conditions, the current sharing error on the primary side of the converter is $\Delta\, i_{pri,rms} = 2.77\%$, whereas, on the secondary side, the CS error in diodes 1 and 4 is $\Delta i_{d1/d4,avg} = 3.56\%$, and the CS error in diodes 2 and 3 is $\Delta\, i_{d2/d3,avg} = 5.08\%$. Thus, the maximum difference in the rectifier currents and transformer primary currents are 5.08% and 2.77%, respectively, which reflects excellent CS in the proposed converter under half-load conditions.

D. Phase-Shedding Ability of the Proposed Converter

Phase-shedding is a key feature of the converter that improves efficiency under light-load conditions, a capability not provided by previous IPOP approaches. As explained in Section IV, the proposed converter achieves phase-shedding when the load is at or below 50% of the power rating. This is done without adding control complexity, simply by stopping the switching of one module. When the load exceeds 50%, both modules are activated, and the currents are equally shared.

Phase-shedding has been verified experimentally in Fig. 10. First, Fig. 10(a) shows the transformer primary currents, the gate-to-source voltage v_{gs4} of switch S_4 in module #2, and the output voltage V_o of the converter. Before phase-shedding, the primary currents are balanced between the constituent modules. When phase-shedding is activated, v_{gs4} turns OFF, and the transformer primary current of module #2 becomes zero ($i_{pri2} = 0$ A). Module #1 now delivers all the power, as reflected in the primary current i_{pri1}. Moreover, the output voltage remains unchanged before and after phase-shedding, demonstrating that the converter achieves phase-shedding without compromising load regulation.

In addition, Fig. 10(b) and (c) show the zoomed-in waveforms of the primary currents before and after phase-shedding, respectively. Fig. 10(b) shows balanced primary currents before phase-shedding, whereas Fig. 10(c) shows the complete phase-shedding ability of the proposed converter when $v_{gs4} = 0$ V and module #2 stops delivering power, with $i_{pri2} = 0$ A.

E. Efficiency Tests of the Proposed Converter

The efficiency of the proposed converter has been measured using a YOKOGAWA WT3000 power analyzer. The part numbers for the MOSFETs, diodes, transformers, and inductor cores used in the efficiency tests are provided in Table III.

First, an efficiency test of a single *LLC* converter using center-tapped rectifier is performed. The results show a peak efficiency of 94.1% at the rated power (400 W). Next, the efficiency of the proposed two-phase *LLC* converter is measured at different power levels. When both phases are switching, the power is well shared between modules #1 and #2, and the peak efficiency is identical to that of the single *LLC* converter module. In this case, the efficiency versus power plot is shown in blue in Fig. 11.

If phase-shedding is considered, the efficiency of the proposed converter must be measured when one of the modules is turned OFF, for loads equal to or below 50% of the power rating. At exactly 50% load, the proposed two-phase converter, with both modules sharing currents, achieve an efficiency of 90.491%. However, after applying phase-shedding to module #2, the efficiency increases to 94.1%, which is the same as in the reference module case with 400 W power rating. This represents an improvement in efficiency of 3.60%. At 25% load, the two-phase converter achieves an efficiency of 86.365%. After applying phase-shedding to module #2, the efficiency increases to 93.182% showing a remarkable improvement of 6.82%. Therefore, the proposed converter with phase-shedding at 50% and 25% load can achieve improvements in efficiency of 3.60% and 6.82%, respectively. The efficiency with phase-shedding is plotted in red in Fig. 11, while the dotted green line shows the combined efficiency plot of the proposed converter.

F. Extension to N-Phases

The proposed converter can be extended to *n*-phases, as depicted in Fig. 12. Additional two-phases can be added with a simple connection between their *LC* branches, denoted as l_{lcx}, where $x = 2, 3 \ldots$.Similar to two-phases discussed, the proposed *n*-phases will achieve excellent CS and PS ability. Regarding the PS ability, considering a four-phases as an example, if one or two-phase are turned-OFF at light-load, the two-*LC* branches will con- tinue sharing currents between them. However, the resonance conditions will remain unchanged, ensuring consistent output voltage, which can be obtained as follows:

$$f_{r,2lc} = \frac{1}{2\pi\sqrt{(C_{r1}||C_{r2})\,(L_{r1}||L_{r2})}} = \frac{1}{2\pi\sqrt{L_r C_r}} = f_r \tag{18}$$

where $f_{r,2lc}$ is the resonance frequency with two-*LC* branches equals to single-*LC* branch resonance frequency f_r. In other words, for *n*-*LC* branches the resonance frequency will remain the same $f_{r,nlc} = f_r$.

VII. Conclusion

This paper presents a two-phase IPOP *LLC* resonant converter with a shared inductor-capacitor branch. The converter achieves excellent CS and PS performance without complex control techniques or additional components. By sharing the

inductor-capacitor resonance branch between two-phases, the following advantages are realized:

1) The power density is improved, as only two passive elements (one inductor and one capacitor) are used in the tank circuits, compared to four in previous designs.
2) Excellent current sharing is achieved under full load, which is critical for thermal distribution. The observed CS error is 2.48% for the primary transformer currents and 2.0% for the rectifier currents, outperforming existing methods.
3) Phase-shedding operation improves efficiency by 3.60% at 50% load and 6.82% at 25% load, demonstrating superior performance over existing CI, CC, and UCICC methods.
4) The proposed CS approach can be extended to more than two or to n-phases with simple connections between the shared branches.
5) A bifilar winding technique is used to mitigate the CS errors in individual converter center-tapped rectifiers.

Notably, the proposed converter is ideal for high step-down applications, providing excellent current-sharing in high-current rectifiers, transformers, and primary switching devices without additional control or components. Its step-down nature ensures that the inductor-capacitor branch handles only part of the total load current, addressing thermal runaway due to high current stress effectively.

REFERENCES

[1] B. Lu, W. Liu, F. C. Lee, and J. D. Van Wyk, "Optimal design methodology for LLC resonant converter," in *Proc. 21st Annu. IEEE Appl. Power Electron. Conf. Expo.*, 2006, pp. 533–538.

[2] B. Yang, "Topology investigation for front end DC-DC power conversion for distributed power system," Ph.D. dissertation, Virginia Polytech. Inst. State Univ., Blacksburg, VA, USA, 2003.

[3] I. O. Lee and G. W. Moon, "The $k - Q$ analysis for an LLC series resonant converter," *IEEE Trans. Power Electron.*, vol. 29, no. 1, pp. 13–16, Jan. 2014.

[4] J. W. Kim, H. S. Choi, and B. H. Cho, "A novel droop method for converter parallel operation," *IEEE Trans. Power Electron.*, vol. 17, no. 1, pp. 25–32, Jan. 2002.

[5] Y. Panov, J. Rajagopalan, and F. C. Lee, "Analysis and design of N parallel DC-DC converters with master-slave current control," *Proc. IEEE Appl. Power Electron. Conf.*, vol. 1, pp. 436–442, 1997.

[6] H. Chen, X. Wu, and S. Shao, "A current-sharing method for interleaved high-frequency LLC converter with partial energy processing," *IEEE Trans. Ind. Electron.*, vol. 67, no. 2, pp. 1498–1507, Feb. 2020.

[7] E. Orietti, P. Mattavelli, G. Spiazzi, C. Adragna, and G. Gattavari, "Two-phase interleaved LLC resonant converter with current-controlled inductor," in *Proc. IEEE Braz. Power Electron. Conf.*, 2009, pp. 298–304.

[8] H. Figge, T. Grote, N. Froehleke, J. Boecker, and P. Ide, "Paralleling of LLC resonant converters using frequency controlled current balancing," in *Proc. IEEE Power Electron. Specialists Conf.*, 2008, pp. 15–19.

[9] K. Murata and F. Kurokawa, "An interleaved PFM LLC resonant converter with phase-shift compensation," *IEEE Trans. Power Electron.*, vol. 31, no. 3, pp. 2264–2272, Mar. 2016.

[10] Z. Hu, Y. Qiu, L. Wang, and Y.-F. Liu, "An interleaved LLC resonant converter operating at constant switching frequency," *IEEE Trans. Power Electron.*, vol. 29, no. 6, pp. 2931–2943, Jun. 2014.

[11] Z. Hu, Y. Qiu, Y.-F. Liu, and P. C. Sen, "A control strategy and design method for interleaved LLC converters operating at variable switching frequency," *IEEE Trans. Power Electron.*, vol. 29, no. 8, pp. 4426–4437, Aug. 2014.

[12] Y. Nakakohara, H. Otake, T. M. Evans, T. Yoshida, M. Tsuruya, and K. Nakahara, "Three-phase LLC series resonant DC-DC converter using SiC MOSFETs to realize high-voltage and high-frequency operation," *IEEE Trans. Ind. Electron.*, vol. 63, no. 4, pp. 2103–2110, Apr. 2016.

[13] M. Noah et al., "A current sharing method utilizing single balancing transformer for a multiphase LLC resonant converter with integrated magnetics," *IEEE J. Emerg. Sel. Top. Power Electron.*, vol. 6, no. 2, pp. 977–992, Jun. 2018.

[14] C. Liu et al., "Magnetic-coupling current-balancing cells-based input-parallel output-parallel LLC resonant converter modules for high-frequency isolation of DC distribution systems," *IEEE Trans. Power Electron.*, vol. 31, no. 10, pp. 6968–6979, Oct. 2016.

[15] U. Ahmad, H. Cha, and N. Naseem, "Integrated current balancing transformer based input-parallel output-parallel LLC resonant converter modules," *IEEE Trans. Power Electron.*, vol. 36, no. 5, pp. 5278–5289, May 2021.

[16] U. Ahmad, H. Cha, and J.-S. Ro, "Integrated current balancing cells based IPOP bidirectional $CLLC$ resonant converter modules for high-power applications," *IET Power Electron*, vol. 15, pp. 1687–1698, 2022.

[17] U. Ahmad, H. Cha, and N. Naseem, "Integrated current balancing transformer-based input-parallel output-parallel LLC resonant converter modules," in *Proc. IEEE 10th Int. Conf. Power Electron., ECCE Asia, S. Korea*, 2019, pp. 1133–1140.

[18] O. Kirshenboim and M. M. Peretz, "Combined multilevel and two-phase interleaved LLC converter with enhanced power processing characteristics and natural current sharing," *IEEE Trans. Power Electron.*, vol. 33, no. 7, pp. 5613–5620, Jul. 2018.

[19] Y. Tada, M. Uno, and Y. Sato, "Three-phase interleaved LLC asymmetric resonant converter with capacitive current balancing and reduced switch voltage stress," *IEEE Access*, vol. 8, no. 1, pp. 5688–5698, 2019.

[20] Y. Yang, J. Yao, H. Li, and J. Zhao, "A novel current sharing method by grouping transformer's secondary windings for a multiphase LLC resonant converter," *IEEE Trans. Power Electron.*, vol. 35, no. 5, pp. 4877–4890, May 2020.

[21] Z. Sun, Q. Wu, Q. Wang, J. Li, and Q. Liu, "An improved grouping transformer's secondary windings current sharing method for multiphase LLC converter," *IEEE Trans. Power Electron.*, vol. 38, no. 8, pp. 9872–9884, Aug. 2023.

[22] H. Dong, X. Xie, S. Xu, and H. Yu, "A novel current sharing scheme for two-phase interleaved LLC converter based on virtual controllable voltage sources," *IEEE Trans. Power Electron.*, vol. 37, no. 2, pp. 1210–1216, Feb. 2022.

[23] T. Shimada, "Current sharing method using secondary voltage ripple for an interleaved LLC resonant converter," in *Proc. 21st IEEE Eur. Conf. Power Electron. Appl.*, 2019, pp. P.1–P.7.

[24] J. Wang, W. Pei, J. Hu, S. Zhao, and J. Zhuang, "Five-phase LLC resonant DC-DC converter utilizing CLC filter for current sharing," *IEEE Trans. Ind. Electron.*, vol. 70, no. 9, pp. 8634–8644, Sep. 2023.

[25] H. Wang, Y. Chen, and Y.-F. Liu, "A passive-impedance-matching technology to achieve automatic current sharing for a multiphase resonant converter," *IEEE Trans. Power Electron.*, vol. 32, no. 12, pp. 9191–9209, Dec. 2017.

[26] H. Wang, Y. Chen, Y.-F. Liu, J. Afsharian, and Z. Yang, "A passive current sharing method with common inductor multiphase LLC resonant converter," *IEEE Trans. Power Electron.*, vol. 32, no. 9, pp. 6994–7010, Sep. 2017.

[27] H. Wang et al., "Common capacitor multiphase LLC converter with passive current sharing ability," *IEEE Trans. Power Electron.*, vol. 33, no. 1, pp. 370–387, Jan. 2018.

[28] Z. Sun et al., "A unified common inductor and common capacitor current sharing method for multiphase LLC converter," *IEEE Trans. Power Electron.*, vol. 37, no. 10, pp. 12182–12196, Oct. 2022.

[29] U. Ahmad and H. Cha, "Coupled inductor-based voltage balancing in dual-output CLL resonant converter for bipolar DC distribution system," *IEEE Trans. Power Electron.*, vol. 38, no. 1, pp. 1262–1274, Jan. 2023.

[30] H. Dong and X. Xie, "Review of current-sharing schemes for multiphase LLC resonant converter," *IEEE Trans. Power Electron.*, vol. 40, no. 1, pp. 1322–1345, Jan. 2025.

[31] U. Ahmad, R. Giral, and C. Olalla, "Two-phase LLC converter with common LC branch for inherent current sharing and phase-shedding ability," in *Proc. IEEE Appl. Power Electron. Conf.*, 2024, pp. 2026–2033.

[32] J.-H. Jung, "Bifilar winding of a center-tapped transformer including integrated resonant inductance for LLC resonant converters," *IEEE Trans. Power Electron.*, vol. 28, no. 2, pp. 615–620, Feb. 2013.